Electronic Supplementary Material (ESI) for Molecular Systems Design & Engineering.

Chiral Transfer in Hydrogen-bonded Liquid Crystals

Florian Malotke [a†], Marco Saccone [ab†], Christoph Wölper [c], Ronald Y. Dong [d], Carl A. Michal [d] and Michael Giese* [a]

[a]Institute of Organic Chemistry, University Duisburg-Essen, Universitätsstraße 7, 45141 Essen, Germany. E-mail: michael.giese@uni-due.de.

[b]Dipartimento di Ingegneria, Università degli Studi di Palermo, Viale delle Scienze, Ed. 6, Palermo 90128, Italy.

[c]Institute of Inorganic Chemistry, University Duisburg-Essen, Universitätsstraße 7, 45141 Essen, Germany.

[d]Department of Physics and Astronomy University of British Columbia, 6224 Agricultural Road, Vancouver, Canada

† These authors contributed equally.

Table of contents

1. Materials and Methods

All compounds which are commercially available, have been used as received without further purification. Mass spectra were recorded on a *Bruker* amazon SL or a MaXis 4G Q-TOF mass spectrometer. ^{1}H-, ^{13}C- and ^{19}F-NMR spectra were recorded in deuterated solvents (Chloroform-*d*, Dimethylsulfoxide-d_6) at room temperature, if not declared otherwise on a *Bruker* Avance DRX. Differential scanning calorimetry thermograms have been recorded using a *Mettler Toledo* DSC 3+/700/866/Argon. Samples were weighed into 40 µl standard aluminium crucibles. The heating and cooling rate was set to 10 K/min. Polarized optical microscopy micrographs were recorded on a *Nikon* Eclipse Ni microscope with crossed polarizers, a *Linkam* heating stage and an *OptixCam* Summit K2 OCS-D3K4-14 camera. Elemental analysis was conducted on Euro EA – CHNSO Elemental Analyser from *HEKAtech GmbH*. Solid state ^{2}H-NMR experiments were performed on a Varian Inova 400 spectrometer using a wide line Apex VT probe. Spectra were collected using a quadrupole echo pulse with 3.7 µs π/2 pulses and a 18 µs echo delay. A 2 s repetition delay and typically 64 acquisitions per temperature were used. Calculations were performed on a desktop computer with an Intel® Core™ i7-8750H Processor, 16 GB RAM and the *CrystalExplorer* program. The model energies were calculated using the option “accurate”. A cluster of molecules within a radius of 3.8 Á from the reference molecules was considered.
See http://130.95.176.70/wiki/index.php/Intermolecular_Interaction_Energies for further details.

2. **Synthetic Protocols**

All Alkoxy-azopyridine and alkoxy-stilbazole derivatives have been synthesized following known procedures.[1–3] First the phenolic precursors (1.0 equivalents) were added to a roundbottom flask together with potassium carbonate (1.5 equivalents) and dissolved in 20-30 ml DMF. Subsequently the corresponding alkyl halides (1.1 equivalents) were then added. The reaction mixture was stirred at 90 °C for 15-20 hours. Afterwards the reaction solution was cooled to room temperature and diluted with ethyl acetate. The mixture was then filtered to remove insoluble contaminants and washed several times with ethyl acetate. The organic phase was first washed with a 5-fold volume excess and then finally once with brine. The organic phase was dried over magnesium sulfate and the solvent was finally removed under reduced pressure. The residue obtained was ultimately purified by column chromatography.

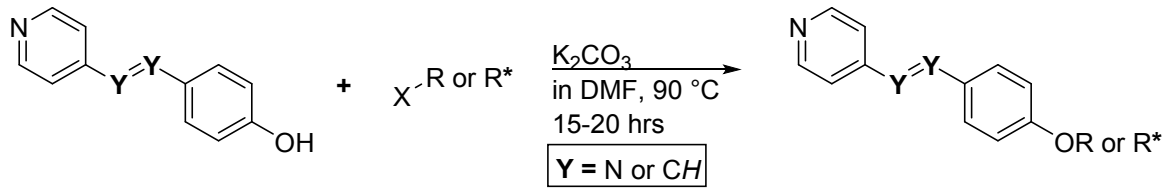

Synthesis of **(*E*)-4-(4-(octyloxy)styryl)pyridine (St-C8)**

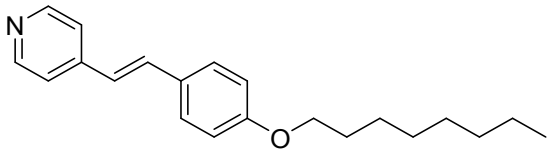

Yield: 4.75 g, 61% (purified from Cyclohexane/ethyl acetate 1:1@SiO2)
^{1}H-NMR (300 MHz, DMSO-d_6, 298 K) δ [ppm]: 8.53 – 8.47 (m, 2H), 7.62 – 7.53 (m, 2H), 7.53 – 7.42 (m, 3H), 7.07 (d, J = 16.5 Hz, 1H), 6.99 – 6.92 (m, 2H), 3.98 (t, J = 6.5 Hz, 2H), 1.70 (p, J = 6.7 Hz, 2H), 1.47 – 1.18 (m, 10H), 0.85 (t, J = 6.7, 3H).

ESI calc. 309.5 [M]; found: 310.2 $[M+H]^+$

Formula $C_{21}H_{27}NO$

Elemental analysis calc. C 81.51%, H 8.79%, N 4.53%; found: C 82.20%, H 8.79%, N 4.62%

Synthesis of **(S,*E*)-4-(4-((3,7-dimethyloct-6-en-1-yl)oxy)styryl)pyridine (St*-Cit)**

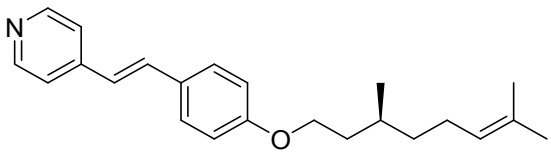

Yield: 3.41 g, 57% (purified from Cyclohexane/ethyl acetate 1:1@SiO2)
^{1}H-NMR (300 MHz, DMSO-d_6, 298 K) δ [ppm]: 8.53 – 8.46 (m, 2H), 7.61 – 7.54 (m, 2H), 7.53 – 7.42 (m, 3H), 7.07 (d, J = 16.5 Hz, 1H), 7.00 – 6.91 (m, 2H), 5.13 – 5.04 (m, 1H), 4.02 (td, J = 6.5, 2.8 Hz, 2H), 1.95 (h, J = 7.4 Hz, 2H), 1.84 – 1.68 (m, 1H), 1.68 – 1.45 (m, 8H), 1.44 – 1.28 (m, 1H), 1.27 – 1.10 (m, 1H), 0.91 (d, J = 6.4 Hz, 3H).

ESI calc. 335.5 [M]; found: 336.3 $[M+H]^+$

Formula $C_{23}H_{29}NO$

Elemental analysis calc. C 82.34%, H 8.71%, N 4.18%, found: C 82.80%, H 8.64%, N 4.30%

Synthesis of **(*E*)-4-((4-(octyloxy)phenyl)diazenyl)pyridine (Ap-C8)**

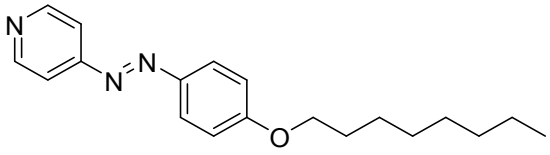

Yield: 4.56 g, 56% (purified from Cyclohexane/ethyl acetate 3:1@SiO2)
^{1}H-NMR (300 MHz, $CDCl_3$-*d*, 298 K) δ [ppm]: 8.79 – 8.72 (m, 2H), 7.98 – 7.89 (m, 2H), 7.69 – 7.62 (m, 2H), 7.04 – 6.95 (m, 2H), 4.03 (t, J = 6.7 Hz, 2H), 1.81 (p, J = 7.0 Hz, 2H), 1.53 – 1.43 (m, 2H), 1.40 – 1.21 (m, 8H), 0.93 – 0.84 (m, 3H).

ESI calc. 311.4 [M]; found: 312.2 $[M+H]^+$

Formula $C_{19}H_{25}N_3O$

Elemental analysis calc. C 73.28%, H 8.09%, N 13.49%; found: C 73.90%, H 7.85%, N 13.30%

Synthesis of **(S,*E*)-4-((4-((3,7-dimethyloct-6-en-1-yl)oxy)phenyl)diazenyl)pyridine (Ap*-Cit)**

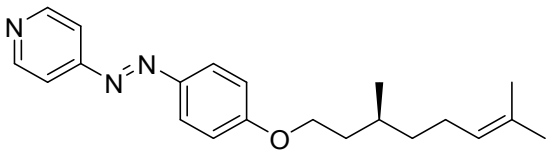

Yield: 4.51 g, 56 % (purified from Cyclohexane/ethyl acetate 3:1@SiO2)
^{1}H-NMR (300 MHz, $CDCl_3$-*d*, 298 K) δ [ppm]: 8.81 – 8.74 (m, 2H), 7.98 – 7.89 (m, 2H), 7.72 – 7.65 (m, 2H), 7.20 – 7.11 (m, 2H), 5.08 (t, J = 7.2 Hz, 1H), 4.13 (td, J = 6.5, 2.8 Hz, 2H), 1.97 (p, J = 7.5 Hz, 2H), 1.78 (dt, J = 12.3, 6.6 Hz, 1H), 1.59 (d, J = 21.6 Hz, 8H), 1.44 – 1.30 (m, 1H), 1.26 – 1.11 (m, 1H), 0.93 (d, J = 6.3 Hz, 3H).

ESI calc. 337.5 [M]; found: 338.3 $[M+H]^+$

Formula $C_{21}H_{27}N_3O$

Elemental analysis calc. 74.74% H 8.06%, N 12.45%; found: C 75.18%, H 7.91%, N 12.18%

Synthesis of **(*E*)-4-((4-(octyloxy)phenyl-2,3,5,6-d_4)diazenyl)pyridine (Ap-C8-d_4)**

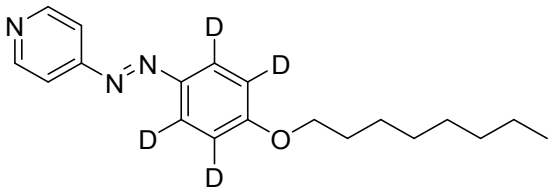

Yield: 1.06 g, 58% (purified from Cyclohexane/ethyl acetate 3:1@SiO2)
^{1}H-NMR (300 MHz, $CDCl_3$-*d*, 298 K) δ [ppm]: 8.80 – 8.75 (m, 2H), 7.71 – 7.67 (m, 2H), 4.06 (t, *J* = 6.6 Hz, 2H), 1.83 (dt, *J* = 15.1, 6.7 Hz, 2H), 1.51 – 1.45 (m, 2H), 1.44 – 1.24 (m, 8H), 0.89 (t, *J* = 6.9 Hz, 3H).

ESI calc. 315.2 [M]; found: 316.1 $[M+H]^+$

Formula $C_{19}H_{21}D_4N_3O$

Elemental analysis calc. C 73.28%, H 8.09%, N 13.49%; found: C 72.95%, H 7.97%, N 13.10%

Synthesis of **(S,*E*)-4-((4-((3,7-dimethyloct-6-en-1-yl)oxy)phenyl-2,3,5,6-d_4)diazenyl)pyridine (Ap*-Cit-d_4)**

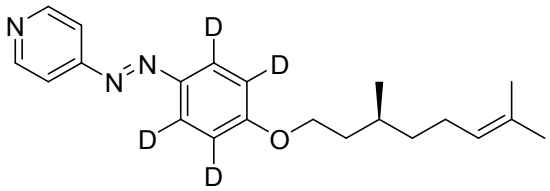

Yield: 0.49 g, 52 % (purified from Cyclohexane/ethyl acetate 3:1@SiO2)
^{1}H-NMR (300 MHz, Chloroform-*d*) δ 8.77 (d, *J* = 6.3 Hz, 2H), 7.69 (d, *J* = 6.3 Hz, 2H), 5.11 (s, 1H), 4.15 – 4.05 (m, 2H), 2.12 – 1.95 (m, 2H), 1.93 – 1.80 (m, 1H), 1.78 – 1.57 (m, 8H), 1.49 – 1.35 (m, 1H), 1.32 – 1.18 (m, 1H), 0.98 (d, *J* = 6.4 Hz, 3H).

ESI calc. 341.5 [M]; found: 342.3 $[M+H]^+$

Formula $C_{21}H_{23}D_4N_3O$

Elemental analysis calc. 74.74% H 8.06%, N 12.45%; found: C 75.12%, H 7.95%, N 12.70%

3.1 Characterisation of hydrogen-bonded liquid crystals

The self-assembled complexes were prepared according to a standard procedure.[4] The core unit and side chain were weighed separately. The individual components were dissolved in acetone, the solutions were combined and ultimately the solvent was removed via a rotary evaporator. Finally, the assembly was thoroughly grinded and dried under vacuum.

The determination of the HTP values was primarily conducted using the *Cano*[5] method (Fig. 1) using polymer-coated wedge cells. Since, in spite of surface coating, a few samples failed to align correctly, these values were inevitably derived from their fingerprint textures. The quality of the alignment depended on the molecular structure of the sample constituents. In particular, fluorine-containing complexes appear to be problematic in alignment, so that fingerprint textures are formed regardless of the surface treatment. The following POM images have been arranged in such a way that the chemical structure of the components of the assembly are depicted first, and then the images, in ascending concentration of chiral dopant between 1-4%.

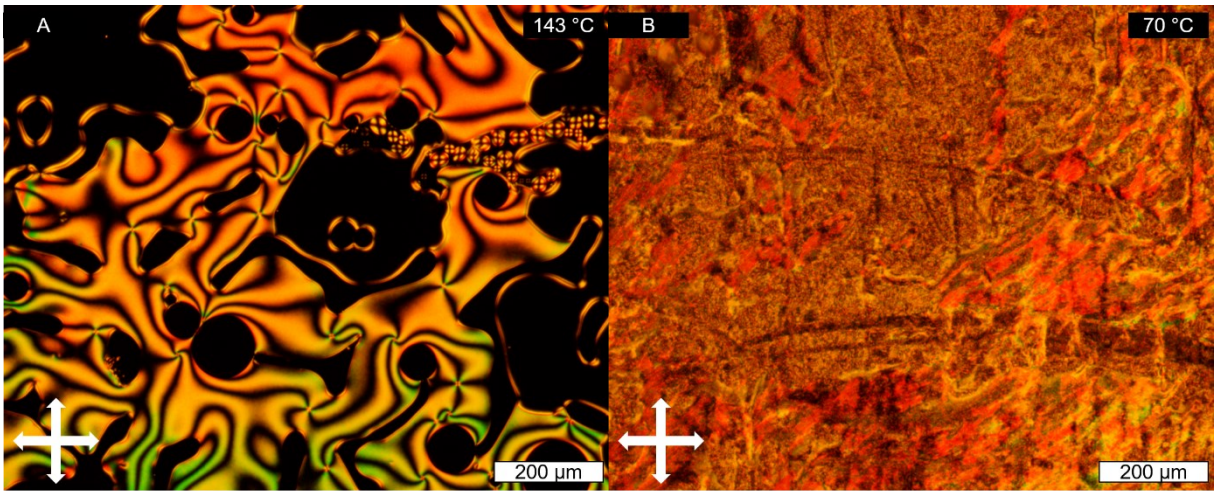

Figure S1: Representative POM images of a nematic phase (A) at 143 °C and a smectic phase (B) at 70 °C for the F-PHG(St_3) complex.

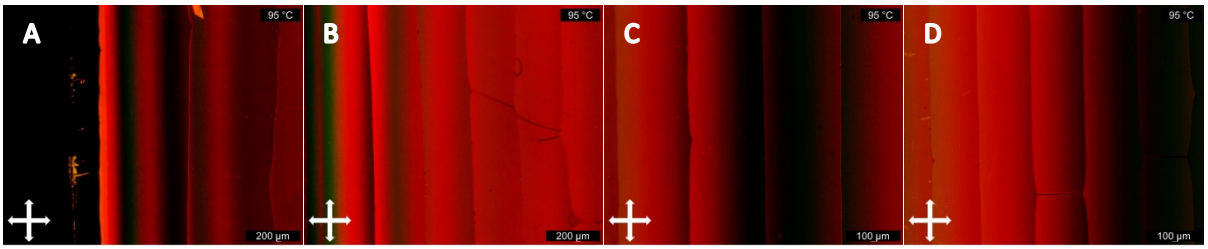

Figure S2: POM images of PHG(1 – 4% Ap*-Cit in Ap-C8) showing its chiral nematic phase at 95 °C under wedge cell conditions (A = 1%, B = 2%, C = 3%, D = 4%).

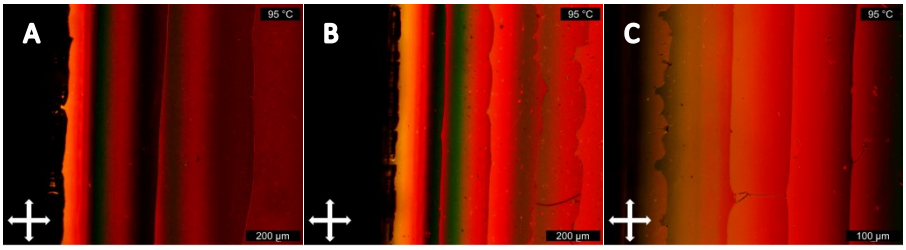

Figure S3: POM images of PHG(1 – 4% St*-Cit in Ap-C8) showing its chiral nematic phase at 95 °C under wedge cell conditions (A = 1%, B = 2%, C = 4%).

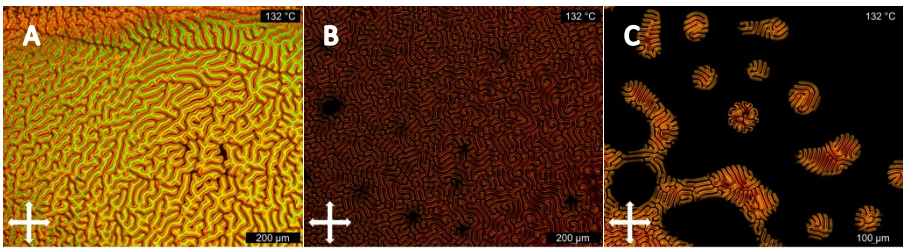

Figure S4: POM images of PHG(2 – 4% Ap*-Cit in St-C8) showing its chiral nematic fingerprint texture at 132 °C (A = 2%, B = 3%, C = 4%).

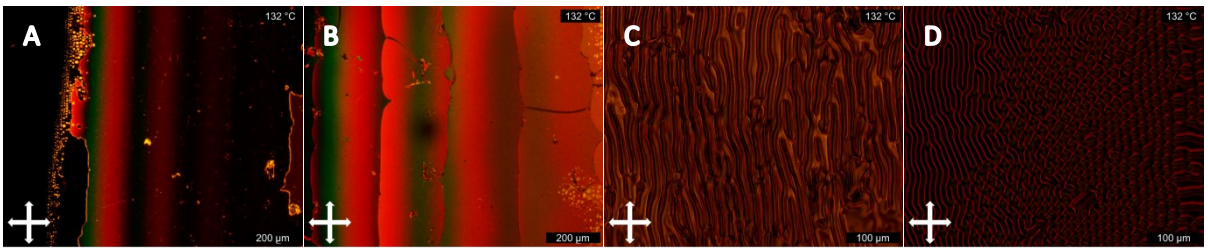

Figure S5: POM images of PHG(1 – 4% St*-Cit in St-C8) weakly showing its chiral nematic phase at 132 °C under wedge cell conditions (A, B) and at 132 °C showing its chiral nematic fingerprint texture (C, D) (A = 1%, B = 2%, C = 3%, D = 4%).

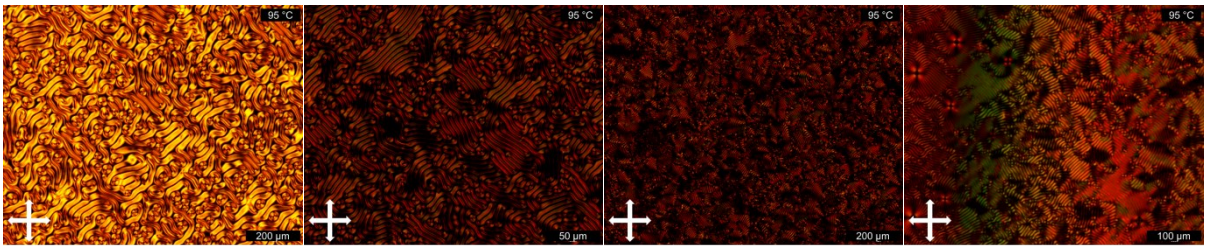

Figure S6: POM image of F-PHG(1 – 4% St*-Cit in Ap-C8) showing its chiral nematic fingerprint texture at 95 °C (A = 1%, B = 2%, C = 3%, D = 4%).

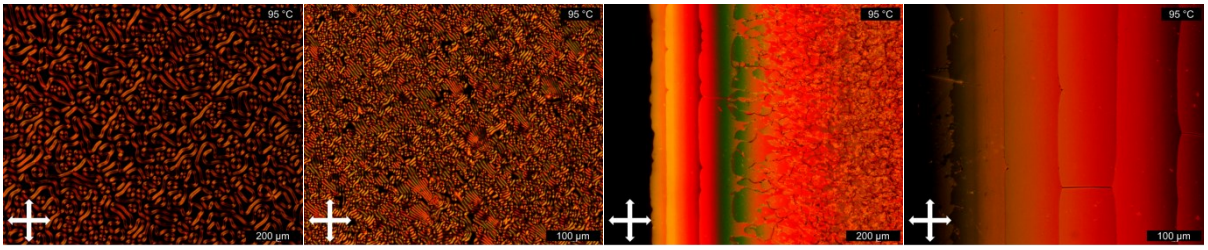

Figure S7: POM image of F-PHG(1 – 4% Ap*-Cit in Ap-C8) showing its chiral nematic fingerprint texture at 95 °C (A, B) and at 95 °C showing its chiral nematic under wedge cell conditions (C,D) (A = 1%, B = 2%, C = 3%, D = 4%).

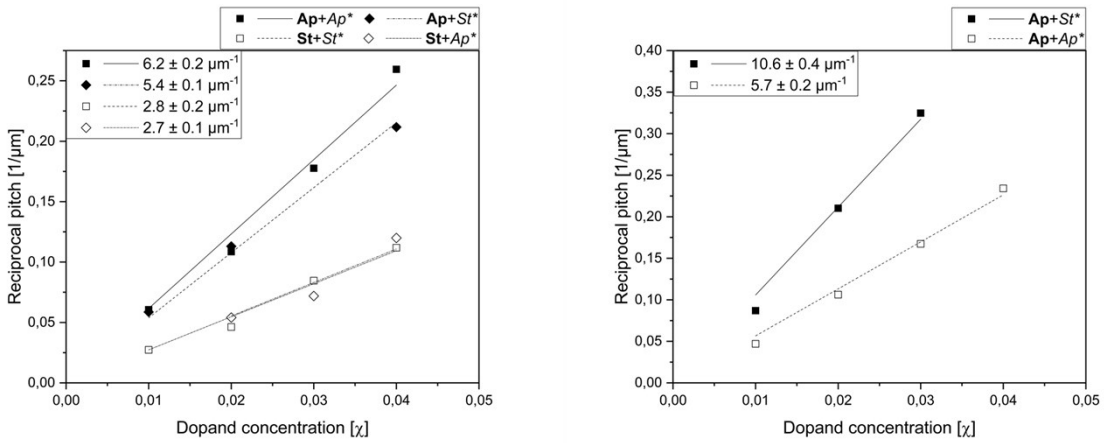

Figure S8: Helical twisting power values obtained for PHG and F-PHG-based HBAs. The achiral hydrogen-bonded assemblies were doped with 1 – 4 mol% of the corresponding acceptor moieties. The helical twisting powers can be found in the top left corner of the corresponding graph.

3.2 **Differential scanning calorimetry for non-chiral HBAs**

The following DSC thermograms show the thermal behaviour of the non-chiral hydrogen bonded assemblies with varying components. Same as for the chiral assemblies a maximum saturation of 1:3 between coreunit and sidechain applies. From top to bottom, the achiral stilbazole ratio increases by substituting the achiral azopyridine component from three equivalents of azopyridine to zero equivalents of azopyridine. The plotted traces are those from the second heating/cooling cycle. The measurements are categorised with respect to core unit used, starting with PHG complexes followed by F-PHG complexes. The heating/cooling ramp was set to constant 10 °C/min.

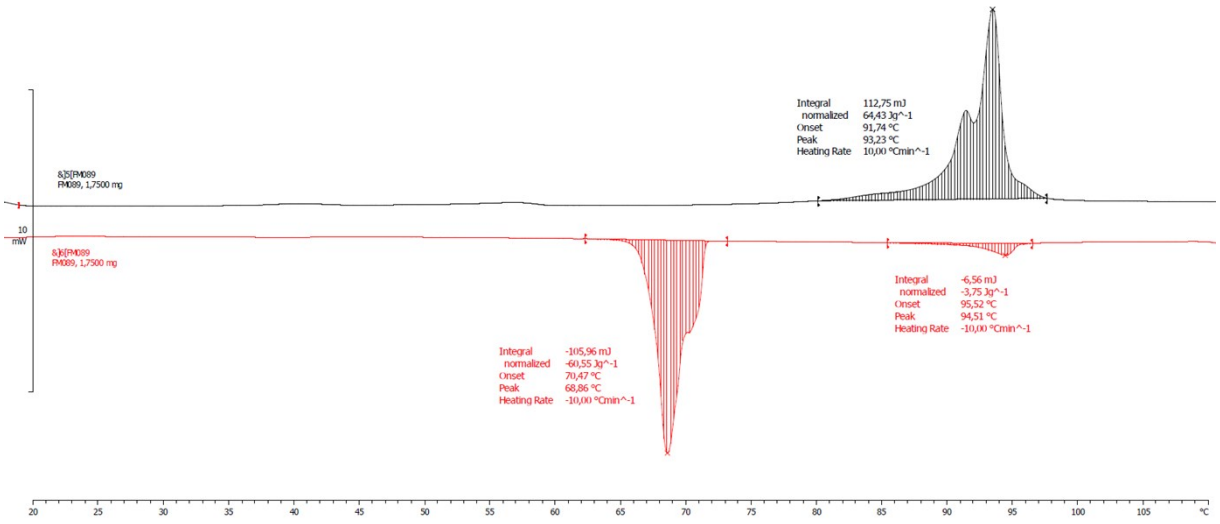

Figure S9: Differential scanning calorimetry traces of PHG(Ap_3) at 10 °C/min

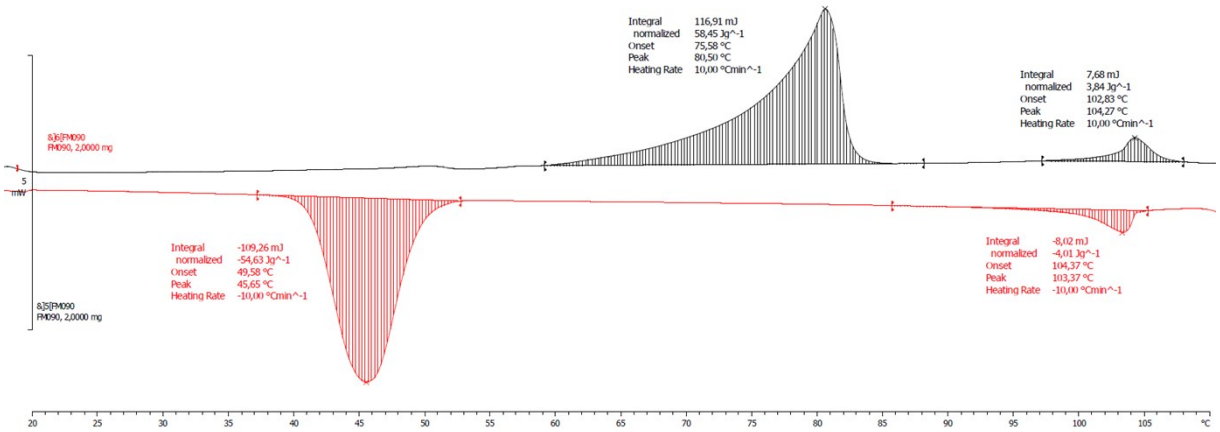

Figure S10: Differential scanning calorimetry traces of PHG(Ap_2St_1) at 10 °C/min

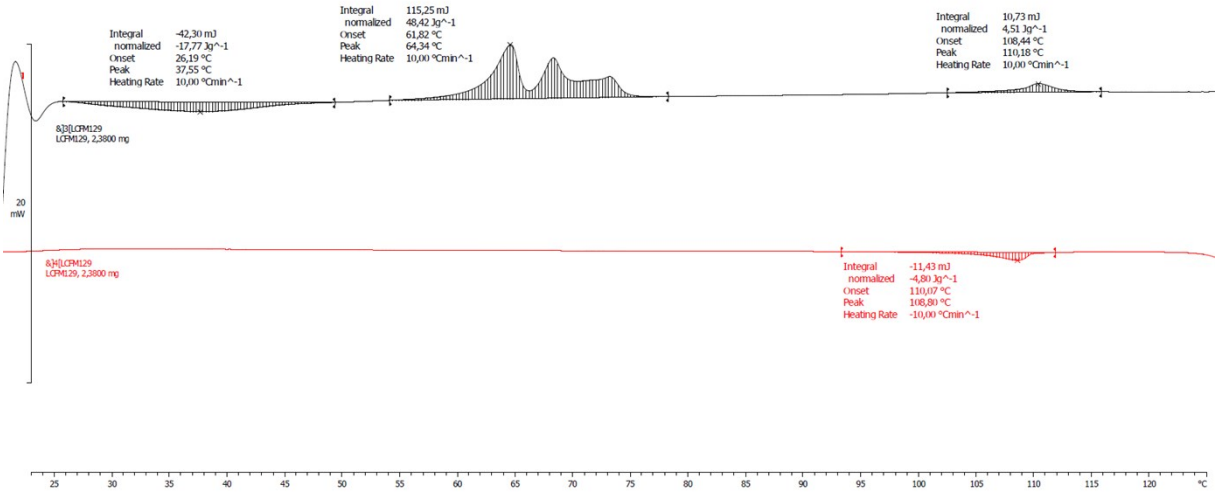

Figure S11: Differential scanning calorimetry traces of PHG($Ap_{1.5}S_{t1.5}$) at 10 °C/min

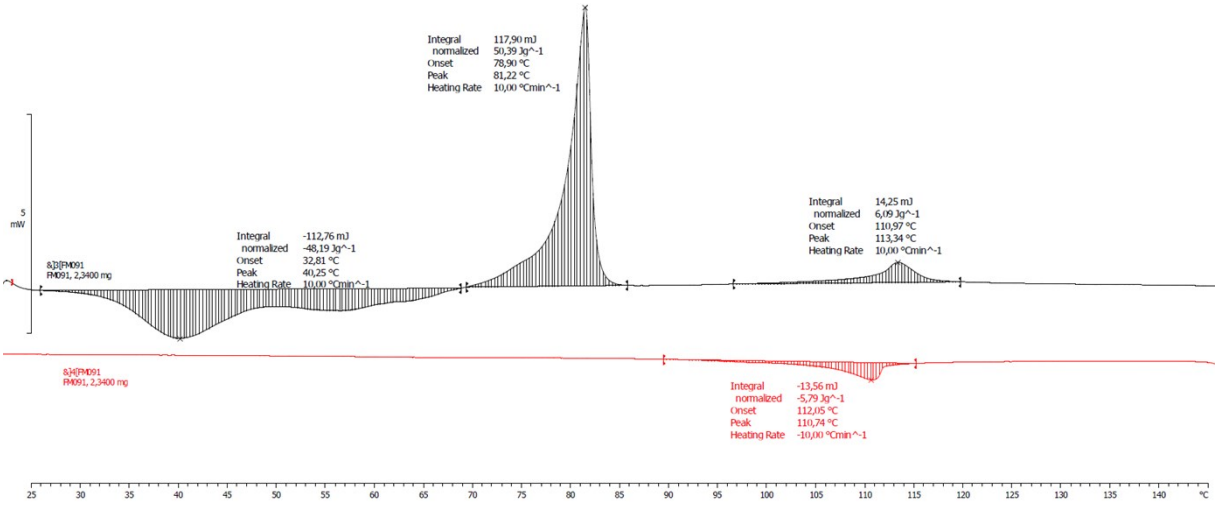

Figure S12: Differential scanning calorimetry traces of PHG(Ap_1St_2) at 10 °C/min

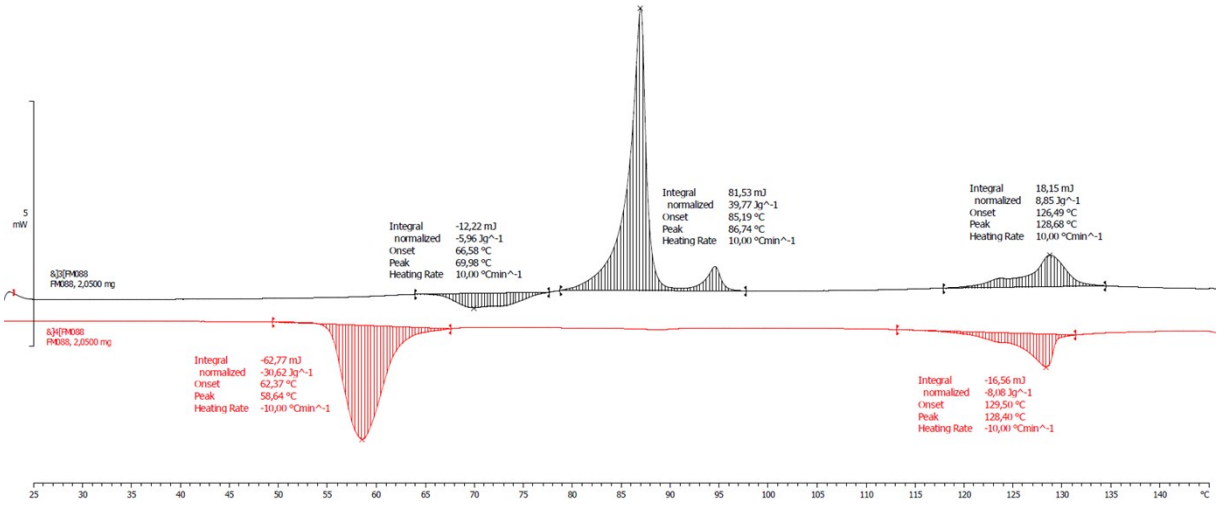

Figure S13: Differential scanning calorimetry traces of PHG(St_3) at 10 °C/min

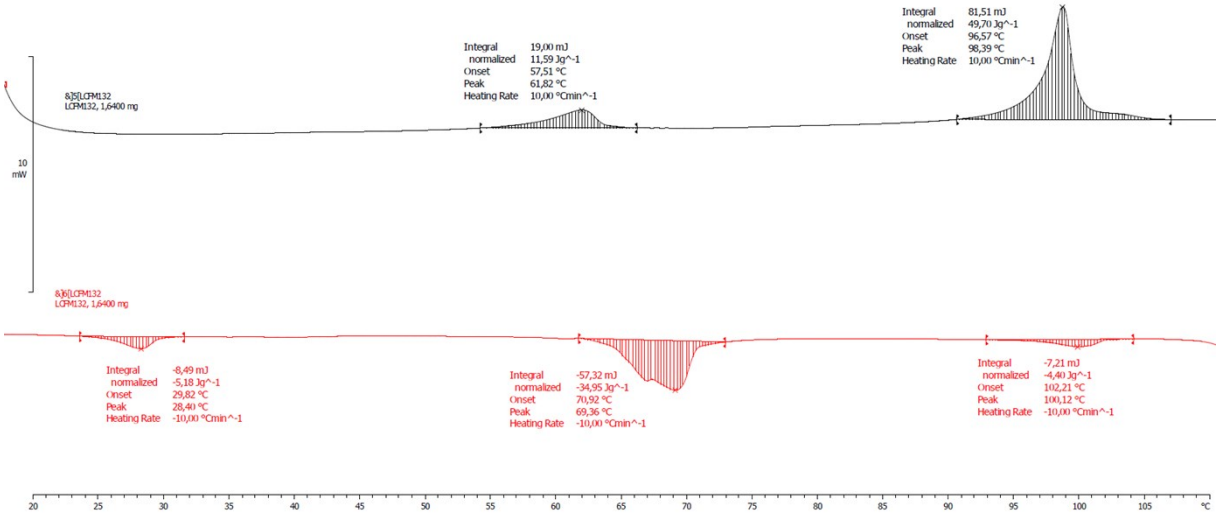

Figure S14: Differential scanning calorimetry traces of F-PHG(Ap_3) at 10 °C/min

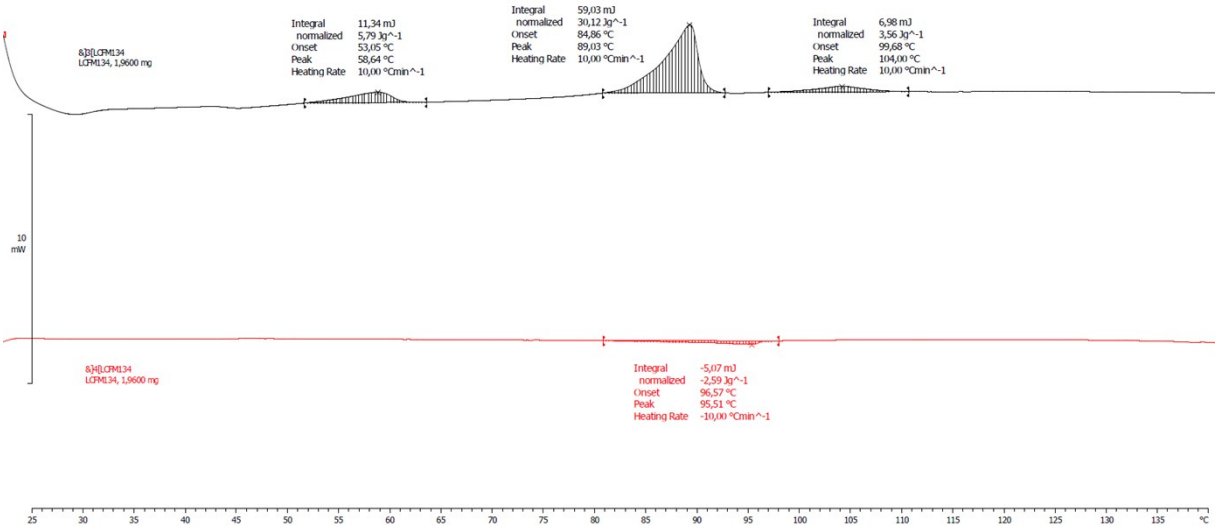

Figure S15: Differential scanning calorimetry traces of F-PHG(Ap_2St_1) at 10 °C/min

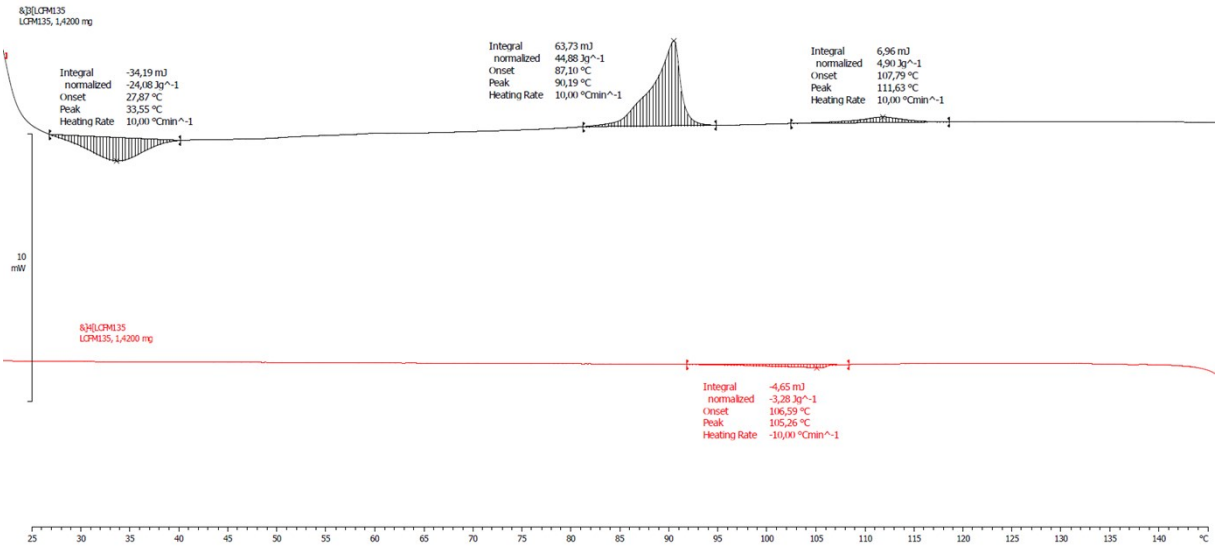

Figure S16: Differential scanning calorimetry traces of F-PHG($Ap_{1.5}St_{1.5}$) at 10 °C/min

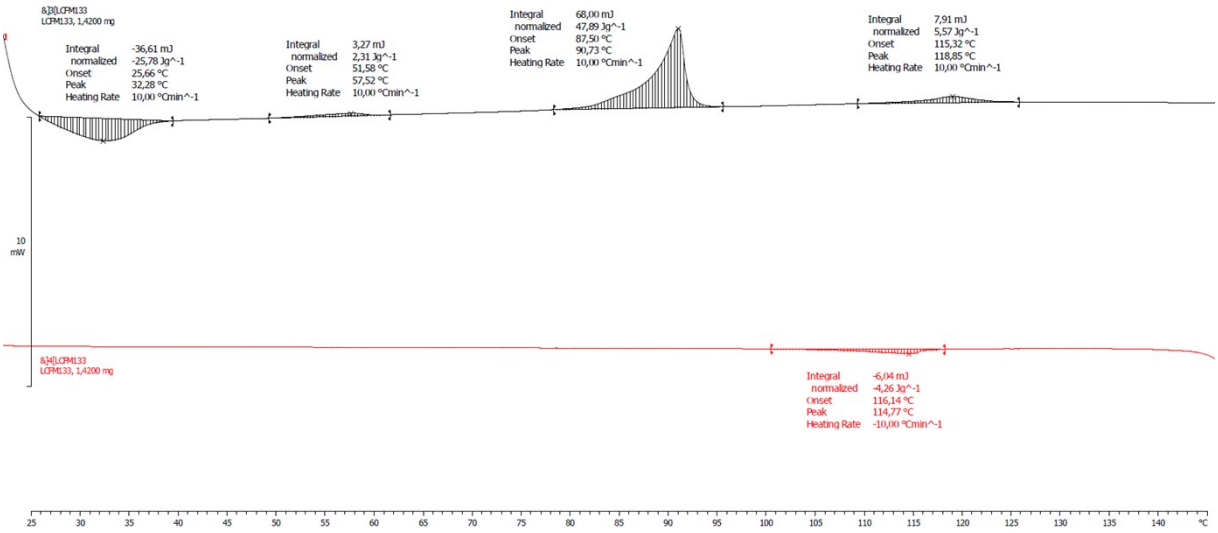

Figure S17: Differential scanning calorimetry traces of F-PHG(Ap_1St_2) at 10 °C/min

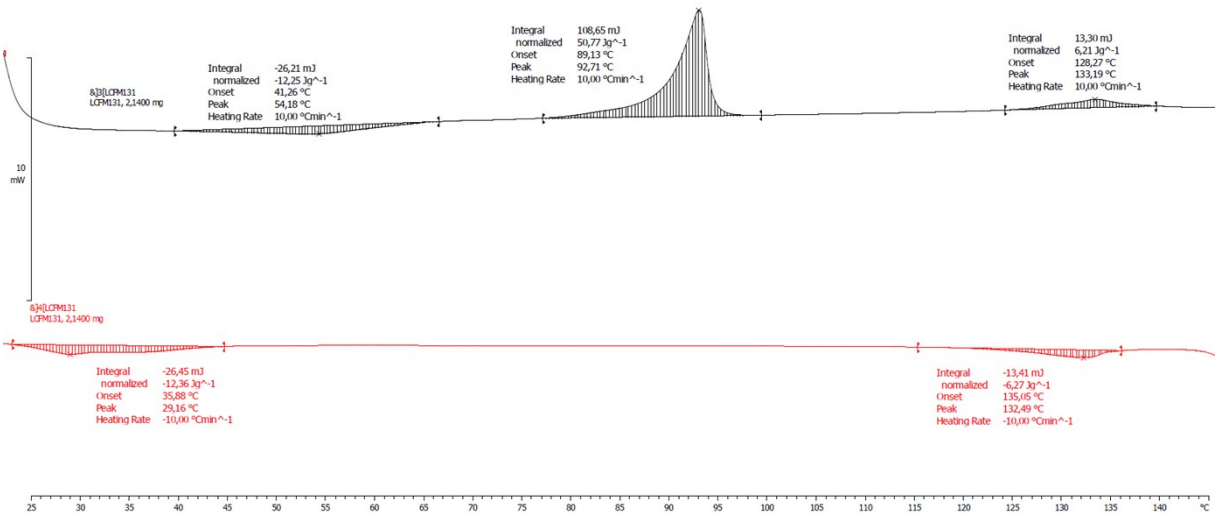

Figure S18: Differential scanning calorimetry traces of F-PHG(St_3) at 10 °C/min

4. Variable-temperature solid-state-NMR studies

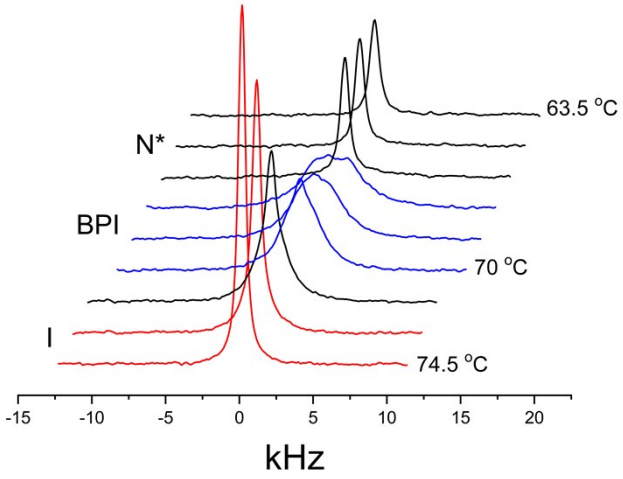

Figure S19: DNMR spectra **of F-PHG(Ap*-d_4)$_{1.5}$(Ap-8)$_{1.5}$** versus temperature at an interval of 1.5 °C.

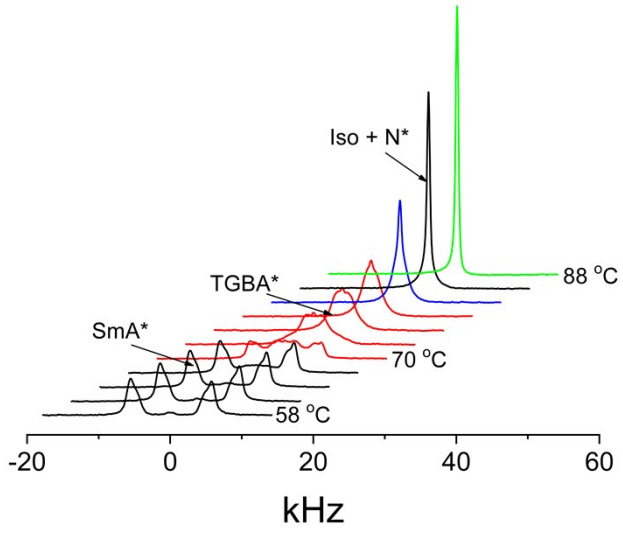

Figure S20: DNMR spectra **of PHG(Ap*-d_4)$_{1.5}$(St-8)$_{1.5}$** versus temperature at an interval of 3.0 °C.

Table S1: List of fitted parameters in the BP I phase

T (°C)	$\langle \nu_q \rangle$ (kHz)	k_j (10^4 s^{-1})	σ (kHz)
70	0.2	4	7
68.5	1.45	2	7.5
67	1.5	2	5.8

Table S2: List of fitted parameters in the TGBA phase. T_2 = 100 ms

T (°C)	$\langle \nu_q \rangle$ (kHz)	k_j (10^4 s^{-1})	σ (kHz)
79	2.0	1.5	1
76	2.45	1.4	1.2
73	2.87	1.1	2
70	3.4	1	2.5

Additional spectral simulations are shown below.

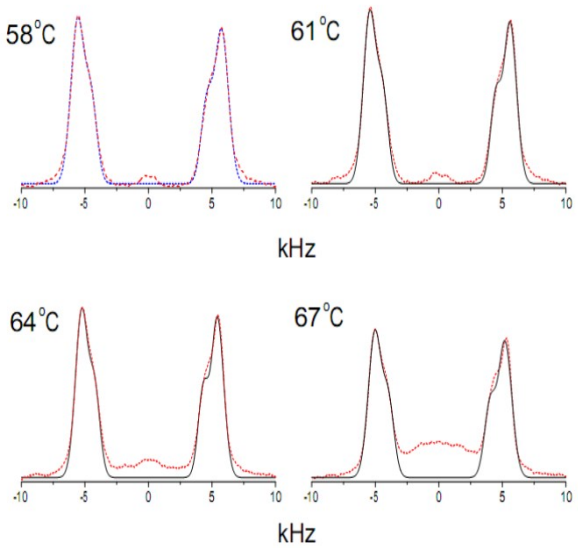

Figure S21: SmA* simulations in PHG(Ap-d_4*$_{1.5}$St$_{1.5}$)

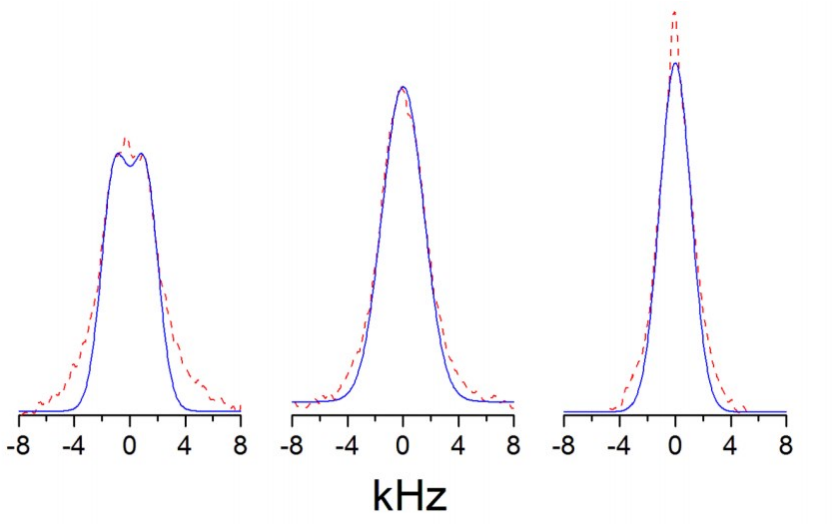

Figure S22: BP I simulations in F-PHG(Ap-d_4*$_{1.5}$Ap$_{1.5}$)

5. Computational studies

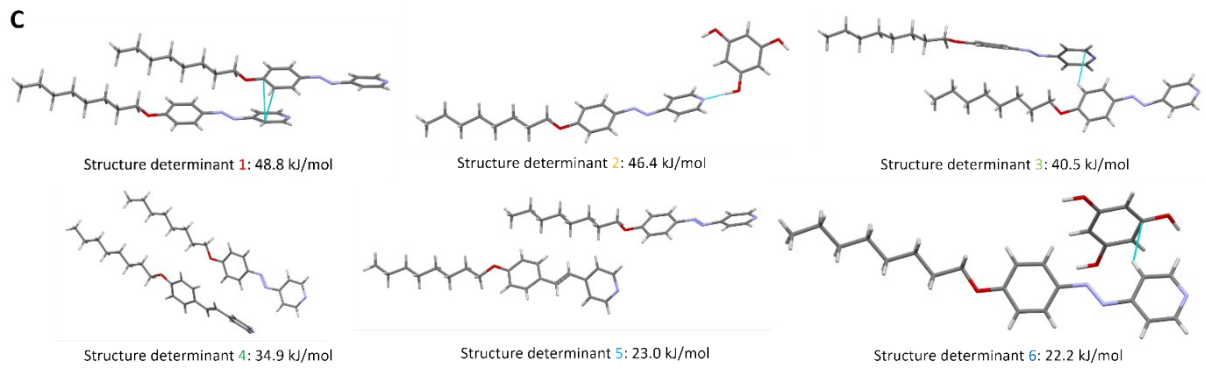

Figure S23: Supramolecular hierarchy of the six most stabilising interactions in the **PHG[(St-8)$_1$(Ap-8)$_2$]** structure (C) as provided by *CrystalExplorer*. The total intermolecular energy is listed for each structure determinant, which shows parts of a pair of two interacting molecules. For each case the structure determinants are arranged in decreasing energy. Blue lines represent short intermolecular contacts below the sum of the van der Waals radii of the respective atoms. Color chart: grey = C, white = H, red = O, blue = N.

PHG[(St-8)$_1$(Ap-8)$_2$]

This structure is almost identical to the former, PHG(Ap-8)$_3$ and features the same structure determinant hierarchy. They only differ in the stabilisation energies of their Structure Determinant 4 (Figures 7B and S23C). Also other small differences are present. The mixed complex features a stronger stabilisation due to the fact that the interaction between the pyridine ring and the stilbene CH group is stronger than the pyridine···azo interaction (see below). The Structure Determinants 6 (Figure 7B and S23C) are very similar and the ranking of interaction energies resembles the pure azopyridine-based boundary case. Accordingly, further permutations show similar behaviour and tendencies with respect to their energy ranking and type of interactions, which is why main emphasis is on the boundary cases.

For a clearer comprehension of chiral induction, theoretical considerations are necessary. As input structures, manually modified crystal structures have been used, all of which have been corrected with respect to their carbon-hydrogen bond. In the following, the most important intermolecular interactions in the solid-state are presented, hereinafter referred to as "structure determinants". On the basis of the crystal structure found for an achiral phloroglucinol-assembly, -CH=CH- has gradually been replaced by -N=N- bonds. These permutations have been studied in detail for their interaction energies and were ranked.

Details on Structure Determinants

Below we give a chart which explain the information given in the ESI Table 1 and 2.

	N	Symop	R	Electron Density	E_ele	E_pol	E_dis	E_rep	E_tot
1	2	3	4	5	6	7	8	9	10

1) Structure Determinant color, as provided in Fig. 5

2) The number of pairs, N, in the graphics window with that energy.

3) Symmetry operator joining the two molecules in the pair.

4) Distance between centers of mass of both molecules (Å).

5) Level of theory at which the electron density is computed: B3LYP/6-31G(d,p) here.

6) Electrostatic contribution (kJ/mol).

7) Polarization contribution (kJ/mol).

8) Dispersion contribution (kJ/mol).

9) Repulsion contribution (kJ/mol).

10) Total energy (kJ/mol): This is the *sum of scaled components* (using the scale factors appropriate to the model as given below), but the *separate components are not scaled*.

Energy Model	**k_ele**	**k_pol**	**k_disp**	**k_rep**
CE-B3LYP. . . B3LYP/6-31G(d,p) electron densities	1.057	0.740	0.871	0.618

Table S3 ***PHG(St-8)$_3$*** energy decomposition

	N	**Symop**	**R**	**Electron Density**	**E_ele**	**E_pol**	**E_dis**	**E_rep**	**E_tot**
	2	x, y, z	8.17	B3LYP/6-31G(d,p)	-10.9	-2.7	-80.2	52.0	-51.2
	1	-	9.38	B3LYP/6-31G(d,p)	-10.8	-2.2	-56.7	35.6	-40.5
	1	-	6.55	B3LYP/6-31G(d,p)	-8.1	-2.4	-31.4	23.7	-23.0
	1	-x, -y, -z	15.70	B3LYP/6-31G(d,p)	-7.6	-2.5	-39.9	36.4	-22.2
	1	-	12.81	B3LYP/6-31G(d,p)	-76.2	-19.1	-16.1	100.9	-46.4
	1	-	5.95	B3LYP/6-31G(d,p)	-8.2	-1.4	-48.2	27.3	-34.9

Table S4 ***PHG(Ap-8)$_3$*** energy decomposition

	N	**Symop**	**R**	**Electron Density**	**E_ele**	**E_pol**	**E_dis**	**E_rep**	**E_tot**
	2	x, y, z	8.17	B3LYP/6-31G(d,p)	-9.7	-2.4	-76.2	47.8	-48.8
	1	-	9.38	B3LYP/6-31G(d,p)	-10.6	-2.2	-54.0	33.3	-39.3
	1	-	6.55	B3LYP/6-31G(d,p)	-5.0	-0.7	-28.4	17.9	-19.4

	1	-	15.70	B3LYP/6-31G(d,p)	-2.4	-2.0	-28.2	19.9	-16.2
	1	-	12.81	B3LYP/6-31G(d,p)	-75.6	-18.2	-16.0	100.5	-45.2
	1	-	5.95	B3LYP/6-31G(d,p)	-3.2	-1.0	-43.3	22.2	-28.2

Table S5 ***PHG[(St-8)$_1$(Ap-8)$_2$]*** energy decomposition

	N	Symop	R	Electron Density	E_ele	E_pol	E_dis	E_rep	E_tot
	2	x, y, z	8.17	B3LYP/6-31G(d,p)	-9.6	-2.3	-76.1	47.7	-48.8
	1	-	9.38	B3LYP/6-31G(d,p)	-10.8	-2.2	-56.7	35.6	-40.5
	1	-	6.55	B3LYP/6-31G(d,p)	-8.1	-2.4	-31.4	23.7	-23.0
	1	-x, -y, -z	15.70	B3LYP/6-31G(d,p)	-7.6	-2.5	-39.9	36.4	-22.2
	1	-	12.81	B3LYP/6-31G(d,p)	-76.2	-19.1	-16.1	100.9	-46.4
	1	-	5.95	B3LYP/6-31G(d,p)	-8.2	-1.4	-48.2	27.3	-34.9

6. Supplementary literature

1. L. Cui and Y. Zhao, *Chem. Mater.*, 2004, **16**(11), 2076.
2. C. Koopmans and H. Ritter, *J. Am. Chem. Soc.*, 2007, **129**(12), 3502.
3. M. Giese, T. Krappitz, R. Y. Dong, C. A. Michal, W. Y. Hamad, B. O. Patrick and M. J. MacLachlan, *J. Mater. Chem. C*, 2015, **3**(7), 1537.
4. M. Saccone, M. Pfletscher, E. Dautzenberg, R. Y. Dong, C. A. Michal and M. Giese, *J. Mater. Chem. C*, 2019, **7**(11), 3150.
5. R. Cano, *Bulletin de la societe francaise mineralogie et de cristallographie*, 1967, **90**(3), 333.